

Rapid Variability in the Japan/East Sea

Basin Oscillations, Internal Tides, and Near-Inertial Oscillations

BY JAE-HUN PARK, D. RANDOLPH WATTS, MARK WIMBUSH,
JEFFREY W. BOOK, KAREN L. TRACEY, AND YONGSHENG XU

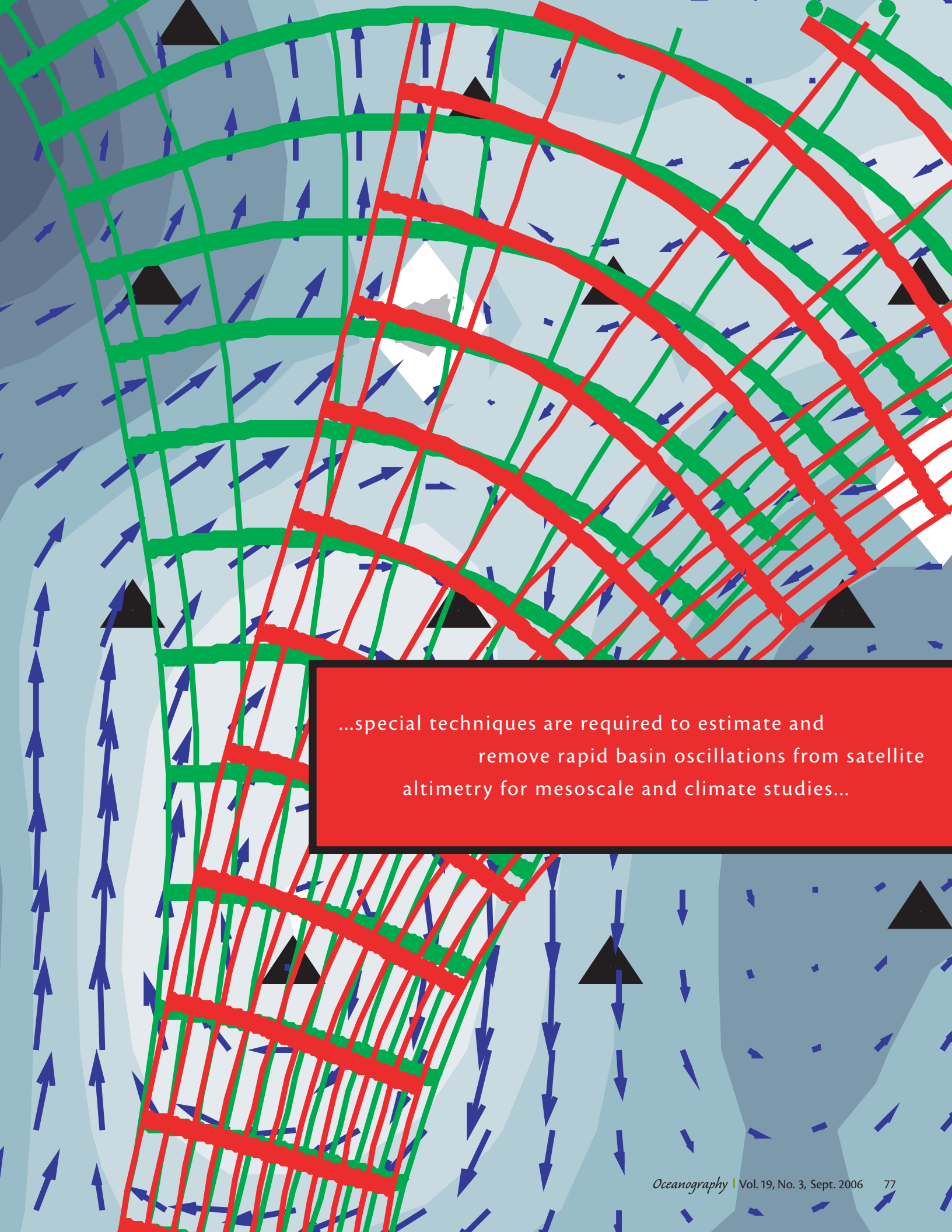
Many processes contribute to the variations of currents, sea surface height (SSH), and thermocline depth in marginal seas. Energetic examples range broadly over time scales from slow mesoscale and interannual variations to rapid basin oscillations, internal tides, and near-inertial oscillations. Our measurement array in the Japan/East Sea (JES) offered a special opportunity to study these processes simultaneously, revealing important interconnections among them.

The PIES (pressure-gauge-equipped inverted echo sounder) experiment in the Ulleung Basin of the southwestern JES was originally designed to investigate the dynamics of meandering currents and eddies in the upper and deep ocean. For those purposes, we low-pass filtered the measurements to examine mesoscale variability. The companion papers by Watts et al. (this issue) and Mitchell et al.

(2005a) describe the mesoscale circulation patterns, including evolution and propagation of warm and cold eddies. The acoustic-echo-time records also included energetic short-period signals, which dominated the bottom pressure record. Within the JES the barotropic (or surface) tidal amplitudes are so small (< 10 cm, compared to 1 m typically in mid-ocean) that these energetic short-period signals stood out and demanded our attention.

We present here an overview of three aspects of short-period variability (less than about 10 days) observed in the JES, even though short-period phenomena were originally outside our main objectives: (1) whole-basin oscillations of SSH with a several-day period, and a method to remove most of their serious aliasing effects upon satellite altimeter measurements; (2) internal tides, which are internal waves generated on the main ther-

mocline by tidal currents crossing the topography at the entrance of the Korea Strait, and which we find are steered in horizontal beams and modulated by the mesoscale currents and eddies inside the JES; and (3) near-inertial oscillations that (surprising us at first) despite their primarily horizontal motion produced variations in the acoustic-echo-time records that could be mapped in relation to the mesoscale eddies and their vorticity distribution. The unifying theme among these findings was the interdependence of long-period and more rapid variability that would commonly occur in marginal seas: (a) special techniques were required to estimate and remove rapid basin oscillations from satellite altimetry for mesoscale and climate studies and (b) long-period mesoscale circulation drastically altered short-period processes, such as internal tides and near-inertial oscillations.



...special techniques are required to estimate and
remove rapid basin oscillations from satellite
altimetry for mesoscale and climate studies...

OBSERVATIONS

As part of the JES initiative by the U.S. Office of Naval Research, an array of PIESs and deep current meters was deployed in the Ulleung Basin from June 1999 to July 2001 (Figure 1). Acoustic sensors recorded hourly echo time for an

acoustic pulse to travel round-trip from the seafloor to the sea surface. As the thermocline changed depth above a PIES, associated changes in temperature caused increases or decreases in acoustic echo time. Acoustic echo time was used to estimate temperature profiles at a suite of

depth levels (Park et al., 2005a,b). Bottom pressure sensors and current meters also recorded hourly data.

BASIN OSCILLATIONS

Marginal seas like the JES may exhibit complicated variations in SSH on a variety of time scales. Temporally tracking and mapping SSH has been the objective of satellite altimetry, which is useful for studying surface geostrophic currents and long-term climate and interannual variability. For these purposes, basin oscillations and tides must be removed very accurately from satellite SSH. If they are not removed, the small residual errors at periods less than the resolved altimeter-sampling period (Nyquist period) of 20 to 70 days can produce a substantial troublesome alias from “trackiness” errors. These errors look like mesoscale eddies (Nam et al., 2004; Xu et al., 2006a) and also features associated with interannual scales (Wunsch and Stammer, 1997). In open-ocean applications, remarkably accurate barotropic models (which use a single layer of constant density) have been developed for tides and response to atmospheric wind stress and pressure forcing—specifically for the purpose of obtaining the residual SSH after removing these short-term fluctuations from the satellite altimetry (Stammer et al., 2000). In contrast, for the JES, tidal models and models of barotropic response to atmospheric forcing have substantial remaining errors, as is likely the case for other marginal seas. Thus, it is of interest to understand the basin response.

At this time, despite great interest, it is very difficult to model the basin barotropic response. The difficulty arises

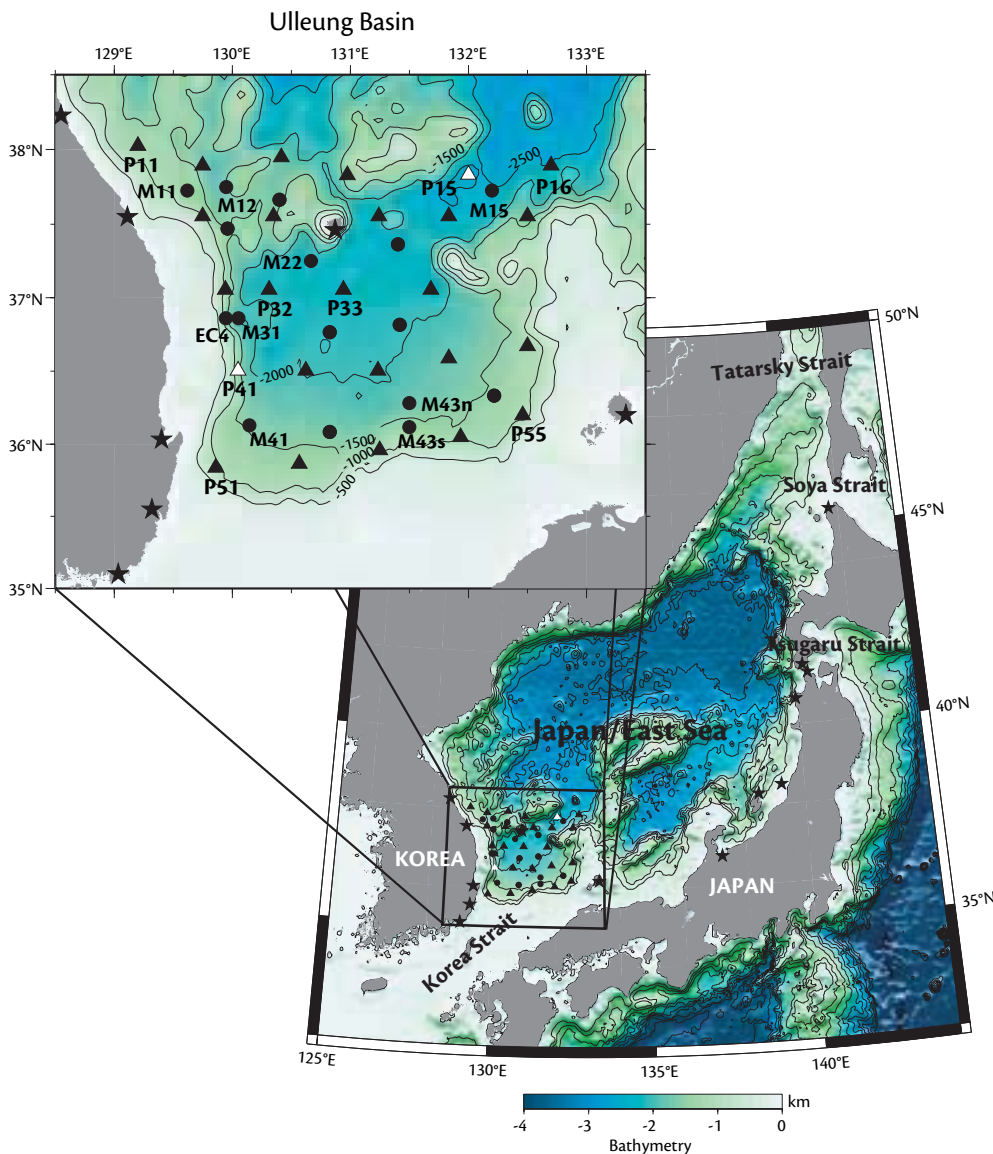


Figure 1. The PIES (black triangles) and current meter (black circles) array in the Japan/East Sea. Coastal tide-gauge stations (stars) were used to estimate subsurface pressure. Open triangles indicate PIES sites where little or no data were obtained. The labeled PIES and current meter sites are discussed in the text. Bathymetry data are from two-minute-resolution global seafloor topography (Smith and Sandwell, 1997) and are contoured at 500-m intervals.

because transports through the straits connecting the JES to the North Pacific Ocean are coupled to both atmospheric forcing and, importantly, to SSH variations in the open ocean caused by mesoscale eddies that impinge outside the straits. Thus, to model the basin barotropic response, one would first need a proven, accurate mesoscale-resolving open-ocean model.

The JES connects to the North Pacific through four straits, all of which have sill depths shallower than 150 m (Figure 1). Because the volume exchange through the Tatarsky Strait is negligible, the Korea, Tsugaru, and Soya Straits govern JES sea-level variations over a broad range of periods. Basin-scale sea-level variations are driven by three main processes: sea-level changes outside the JES; along-strait wind stress; and atmospheric pressure loading on the JES. These processes all drive volume transport variations through the straits (Lyu and Kim, 2005; Xu et al., 2006a).

“Inverted barometer response” is the name applied to an ideal change of SSH in response to local fluctuations of atmospheric pressure to produce zero change in subsurface pressure. This vertical adjustment implies lateral adjustment (not compression) of water volumes. In the open ocean, the water is free to adjust to atmospheric pressure changes, and so it typically exhibits a nearly perfect inverted barometer response. In contrast, semi-enclosed marginal seas may exhibit unique short-period departure from inverted barometer response, because their straits restrict the volume flow. In general, for sufficiently long-period changes in atmospheric pressure, the water volume has enough time to exchange through

their straits and the basin interior maintains the inverted barometer response. In contrast, for processes with periods shorter than the natural period of the basin, about three days in the JES (Lyu et al., 2002), the interior sea level has insufficient time to adjust because the water mass exchange through the straits is restricted. For example, tidal currents through the straits are large, yet the diurnal and semidiurnal tide amplitudes inside the JES are quite small. Additionally, near the natural frequency, the sea-level response can resonate with atmospheric pressure forcing, called a Helmholtz resonance (Garrett, 1983; Lyu et al., 2002; Park and Watts, 2005a).

Our first impression upon plotting the pressure records from the JES was that the same data file had accidentally been used repeatedly—all 23 time series looked nearly identical! The upper panel of Figure 2 shows records from five sites spanning the Ulleung Basin. Correlation coefficients calculated between pairs of sites exceeded 0.95, even for sites separated by distances up to 350 km. The bottom pressure records exhibited short-period variations equivalent to 10–20 cm in sea level at time scales of 2–15 days. Their variance-preserving power spectra peaked broadly near five-day periods (red line in the lower panel of Figure 2), in the same band as the atmospheric “synoptic-scale” pressure forcing on the Ulleung Basin (green line). In contrast, note how different the bottom pressure response is in the open North Pacific Ocean at a nearby site (black line; 35.6°N, 148.4°E, during 2004–2005). Although that open-ocean site has similar atmospheric pressure forcing, its bottom pressures exhibit virtually no

response at periods shorter than 10 days (like the inverted barometer), whereas there is high energy at mesoscale periods of 20–50 days.

It simplifies matters that the JES is deep, because the effective wavelength of oscillations with periods longer than two days greatly exceeds the basin dimensions. Xu et al. (2006b) have shown that internal basin modes have periods of seven hours or less. Hence, barotropic oscillations of periods longer than two days are uniform and in phase throughout the basin; this uniformity accounts for the observed “common mode” among all the pressure records shown in Figure 2. Thus, we can easily determine the basin barotropic oscillations during our two-year observational period. For example, Teague et al. (2005) remove the common mode from the bottom pressure records to map the deep circulation with highs and lows about a factor of ten smaller than the common mode.

Jae-Hun Park (jpark@gso.uri.edu) is Research Scientist, Graduate School of Oceanography, University of Rhode Island, Narragansett, RI, USA. **D. Randolph Watts** is Professor, Graduate School of Oceanography, University of Rhode Island, Narragansett, RI, USA. **Mark Wimbush** is Professor, Graduate School of Oceanography, University of Rhode Island, Narragansett, RI, USA. **Jeffrey W. Book** is Physical Oceanographer, Naval Research Laboratory, Stennis Space Center, MS, USA. **Karen L. Tracey** is Research Specialist, Graduate School of Oceanography, University of Rhode Island, Narragansett, RI, USA. **Yongsheng Xu** is Ph.D. Candidate, Graduate School of Oceanography, University of Rhode Island, Narragansett, RI, USA.

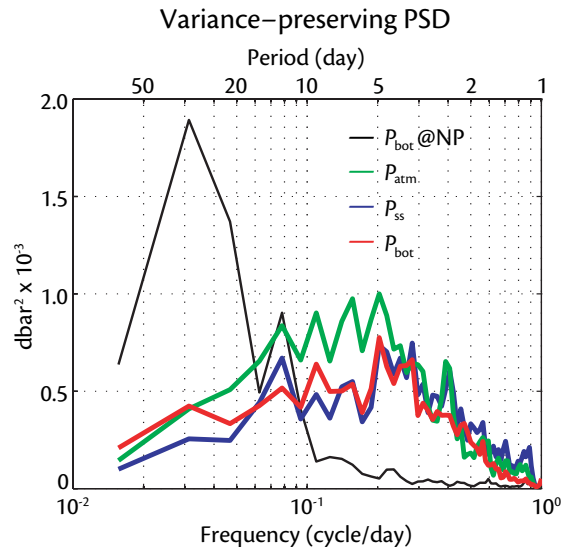
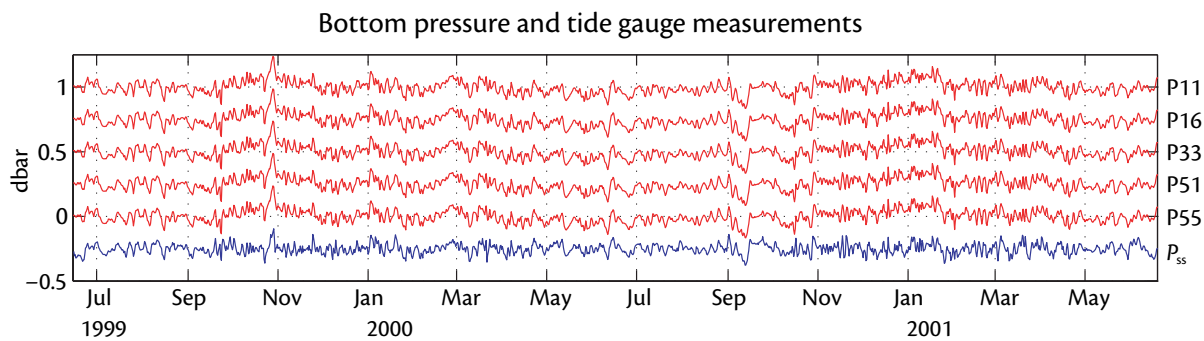


Figure 2. (Upper panel) Time series of bottom pressure (red lines) measured at five sites in the Ulleung Basin appear remarkably similar during the two-year experiment from June 1999 to June 2001. Additionally, the mean subsurface pressure (blue line) calculated from 14 coastal tide-gauge stations closely resembles the bottom pressures. (Lower panel) Variance-preserving power spectra of mean bottom pressure of the five sites (P_{bot} , red line) and mean subsurface pressure (P_{ss} , blue line) within the JES exhibit high energy in the 5–10 day period band. In contrast, little energy occurs in that same period band for a one-year bottom pressure record collected in the North Pacific near 35.6°N, 148.4°E ($P_{bot@NP}$, black line). Also shown is the power spectrum for atmospheric pressure averaged over the Ulleung Basin (P_{atm} , green line). The 95 percent confidence factors are (0.69, 1.60) for P_{bot} , P_{ss} , and P_{atm} , and (0.60, 2.00) for $P_{bot@NP}$.

Using bottom pressure signals is the best way to identify and remove the basin oscillations from satellite altimetry in the JES. However, it would be of great interest to estimate and remove these oscillations for time periods other than 1999–2001. Xu et al. (2006a) show that coastal tide gauges could be used for this purpose. Figure 1 shows 14 stations whose records are less affected by extraneous local fluctuations in sea level such as wind setup. A common mode proxy is generated by averaging together these coastal tide-gauge records, subtracting the local atmospheric pressure at each tide-gauge station, and high-pass filtering (70 days) to remove long-period warming or cooling effects on coastal

sea level. These calculations show that 78 percent of the basin oscillation variance could be estimated for removal from satellite SSH.

INTERNAL TIDES

Surface tides in the JES are about ten times smaller than those of the neighboring Yellow and East China Seas. Figure 3 shows the M_2 semi-diurnal tidal ellipses, superimposed on the co-tidal and co-range chart for the Korea Strait and Ulleung Basin regions. A model that assimilates measurements (Griffin and Thompson, 1996) was used to create Figure 3. Compared to the other tidal constituents (not shown), the M_2 is the dominant tide in the Korea Strait and the

Ulleung Basin. In addition, tidal currents in the Korea Strait are about ten times larger than those inside the Ulleung Basin because the bottom depths differ greatly. Where the strong M_2 tidal currents interact with the shelf break exiting the Korea Strait (see Figure 1), substantial semi-diurnal internal tides with vertical displacements of 20 m (13 percent of the mean thermocline depth of ~ 150 m) are generated. These tides propagate into the JES.

Until now, most internal-tide studies from observations have focused on two-dimensional propagation of waves in (x, z) space, where the x-axis is along the propagation direction and the z-axis is vertical. Usually, variations along the

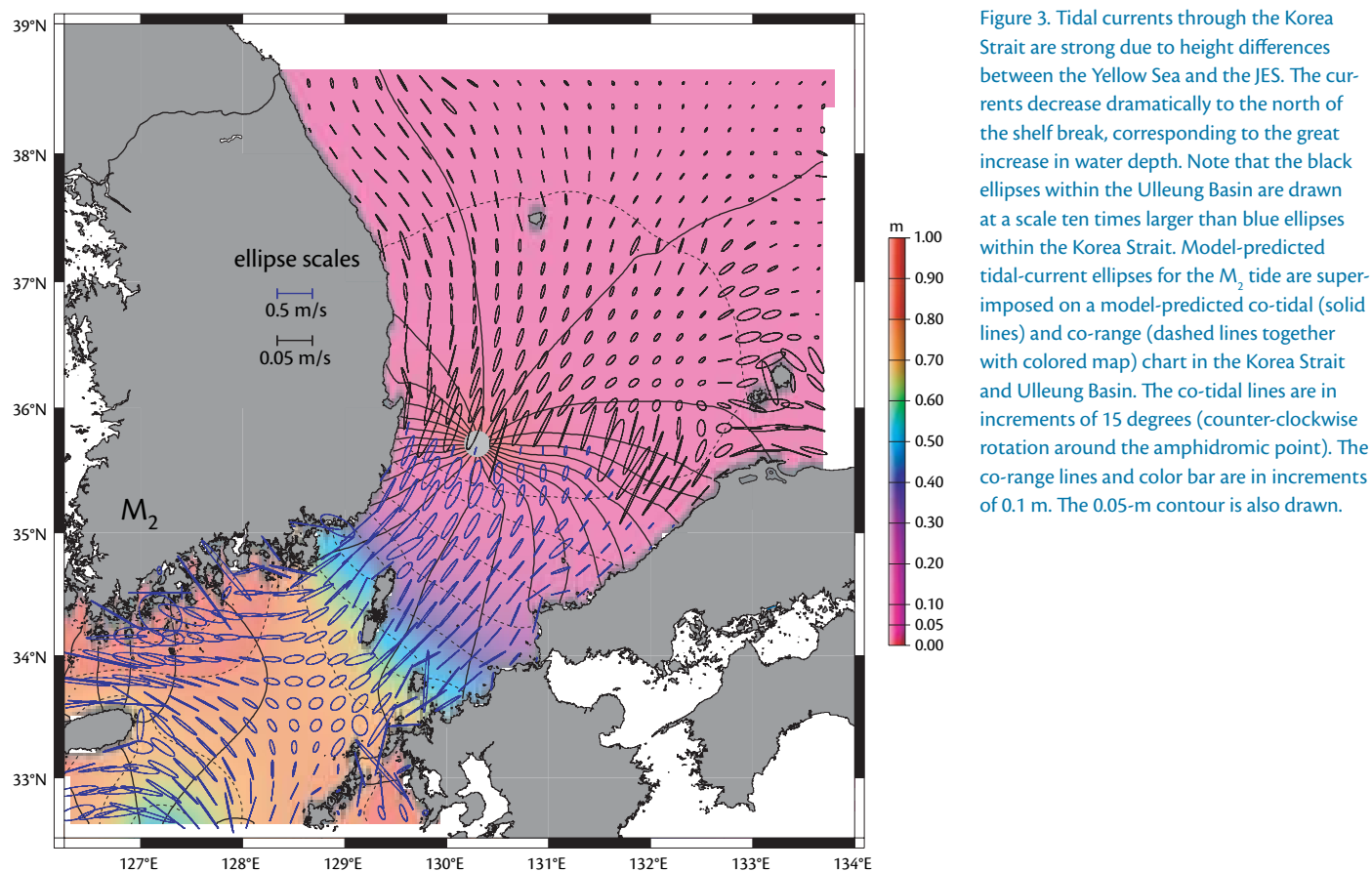


Figure 3. Tidal currents through the Korea Strait are strong due to height differences between the Yellow Sea and the JES. The currents decrease dramatically to the north of the shelf break, corresponding to the great increase in water depth. Note that the black ellipses within the Ulleung Basin are drawn at a scale ten times larger than blue ellipses within the Korea Strait. Model-predicted tidal-current ellipses for the M_2 tide are superimposed on a model-predicted co-tidal (solid lines) and co-range (dashed lines together with colored map) chart in the Korea Strait and Ulleung Basin. The co-tidal lines are in increments of 15 degrees (counter-clockwise rotation around the amphidromic point). The co-range lines and color bar are in increments of 0.1 m. The 0.05-m contour is also drawn.

y-axis, across the propagation direction, have been neglected. However, horizontal propagation of internal tides may be altered significantly through interactions with background currents and eddies.

The PIES array provided a means to study internal-tide propagation in all three dimensions. Because acoustic echo-time variations are mainly caused by vertical displacements of the main thermocline (Watts and Rossby, 1977), vertical thermocline displacements caused by internal tides can be detected by PIES instruments. However, for acoustic echo times to be used for this purpose, it is necessary to accurately measure and remove the surface tides from them (Cartwright, 1982). Bottom pressures mea-

sured by the PIES provided the required surface tide signals.

Using the echo times measured by the PIES array in the JES, Park and Watts (2006) observed the propagation of the first-mode internal tides in the Ulleung Basin. They found that the internal tides propagated from the shelf break near the Korea Strait into the central Ulleung Basin as a laterally restricted “beam.” Most interesting was the fact that the beams were steered and focused in a predictable manner by the background currents and eddies that they encountered.

Figure 4 shows how the internal tide energy distribution changes when the mesoscale circulation changes. Two different time periods are illustrated.

Lunar-monthly (29.5 days) averages of the circulation, indicated by mean 5°C isotherm depth Z_5 , are mapped in the upper row. In the middle row, the internal tide amplitude η_5 within the semi-diurnal band (11.50–12.92 hours) is mapped over the lunar month. The two time intervals compare two complete cycles of spring neap-tide modulation.

During 9/13/99–10/12/99 (Figure 4, left column), the Ulleung Warm Eddy, centered near 36°N, strengthens and starts to merge with a warm eddy to its north, whose southern part appears near 38°N in the Z_5 map. The semi-diurnal internal-tide beam (dark red and orange in the middle panel of Figure 4) refracts significantly eastward as the internal

tides encounter the developed Ulleung Warm Eddy during this month.

During 1/9/00–2/7/00 (Figure 4, right column), the Ulleung Warm Eddy is even more strongly developed, centered in the Z_5 map near 37.5°N, 131°E. However, the internal tide beam first encounters a cold eddy (Dok Cold Eddy) that is located to its southwest (Mitchell et al., 2005b).

The semi-diurnal internal-tide beam refracts westward during this lunar month when the cold eddy is located to the west of the beam (middle panel). Note that at locations like 37.5°N, 132.5°E or along the shelf break off Korea, internal tide amplitude η_5 varies by a factor of two from one lunar month to the other in response to these refraction pattern

changes. The monthly average Z_5 and η_5 maps in Figure 4 demonstrate that mesoscale eddies located in the path of the propagating internal tides cause eastward or westward refraction.

The green and red lines in the lower row of panels in Figure 4 are superimposed on the phase-speed field of the first-mode baroclinic semi-diurnal in-

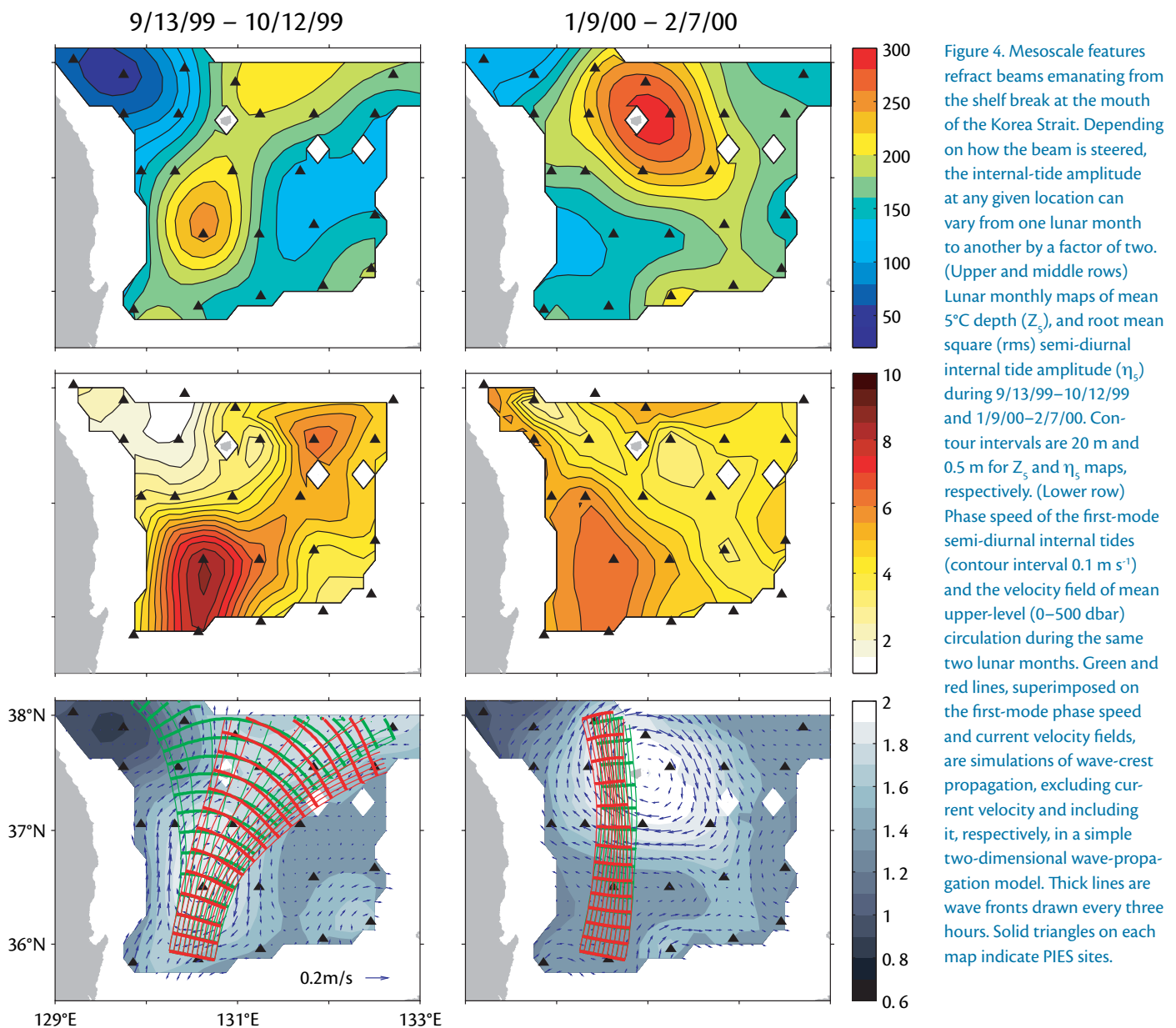


Figure 4. Mesoscale features refract beams emanating from the shelf break at the mouth of the Korea Strait. Depending on how the beam is steered, the internal-tide amplitude at any given location can vary from one lunar month to another by a factor of two. (Upper and middle rows) Lunar monthly maps of mean 5°C depth (Z_5), and root mean square (rms) semi-diurnal internal tide amplitude (η_5) during 9/13/99–10/12/99 and 1/9/00–2/7/00. Contour intervals are 20 m and 0.5 m for Z_5 and η_5 maps, respectively. (Lower row) Phase speed of the first-mode semi-diurnal internal tides (contour interval 0.1 m s⁻¹) and the velocity field of mean upper-level (0–500 dbar) circulation during the same two lunar months. Green and red lines, superimposed on the first-mode phase speed and current velocity fields, are simulations of wave-crest propagation, excluding current velocity and including it, respectively, in a simple two-dimensional wave-propagation model. Thick lines are wave fronts drawn every three hours. Solid triangles on each map indicate PIES sites.

ternal tides and the velocity field of mesoscale circulation. They illustrate the propagating wave fronts and rays simulated in two ways. A simple geometric optics model (Sherwin et al., 2002) was used to simulate the propagation of the internal wave fronts. First, the simulation was conducted without including the current field in the simulation to isolate the effect of stratification on the refraction (green lines). Second, the simulation included both the first-mode internal tide phase speed and the current field to illustrate the additional effect of current shear (red lines). The simulated results for both model versions capture qualitatively the observed refraction patterns of the internal tide beam for the two lunar months (middle panels in Figure 4). More examples are discussed in Park and Watts (2006). These simulation results illustrate the essential roles of both mesoscale circulation stratification and horizontal current shear on internal tide energy propagation.

NEAR-INERTIAL OSCILLATIONS

In the northern hemisphere on a rotating Earth (and in the absence of other forces), a current of water set into motion would feel the Coriolis force perpendicular to the flow, ever turning it to the right. This effect creates circular motions called inertial oscillations. The inertial period varies with latitude such that inertial oscillations at higher latitudes have shorter periods. At 37°N, roughly the middle latitude of the PIES array in the JES, the inertial period is 19.9 hours. The spectral energy peak calculated for measured currents is very close to the local inertial frequency, but differs slightly and generally occurs at

slightly higher frequencies. Because of this very small frequency shift, they are usually referred to as near-inertial oscillations. The energy associated with near-inertial oscillations propagates from the sea surface to the ocean bottom, and it also travels equatorward of the source region (Garrett, 2001).

Inertial-oscillation currents are nearly horizontal. Thus, we did not at first expect to observe them with our PIES instruments, because changes in acoustic echo time arise from vertical displacements of the thermocline. Yet, near-inertial motions have frequencies slightly higher than the local inertial frequency, which tilts the oscillations very slightly from horizontal (on the order of 10^{-3} rad). A near-inertial motion several kilometers in diameter tilted by this tiny angle produces a vertical thermocline displacement of several meters, readily measurable by the PIES. Park and Watts (2005b) demonstrated that acoustic-echo-time measurements could be used to analyze motions in the inertial frequency band. They demonstrated that time series of band-pass-filtered acoustic echo time at the local inertial frequency band have higher energy during wintertime associated with the stronger winter winds. In addition, they found that the near-inertial energy differed among the sites and demonstrated how the mesoscale current field governed its distribution, as follows.

Mesoscale currents affect the distribution of near-inertial wave energy because their lateral shear modifies the local inertial frequency. The current shear can trap and refract near-inertial wave energy, as has been described in several studies. Kunze (1985) shows, for example, that

near-inertial wave energy can be trapped in a northern-hemisphere region of negative relative vorticity, which creates a waveguide by shifting the lowest internal wave frequency from the exact local inertial frequency to a lower effective inertial frequency. This region functions like a near-inertial waveguide because oscillations at slightly subinertial frequency are supported as internal waves within it but not outside it—hence they cannot propagate out of the region. Examples of negative relative vorticity regions in the ocean are clockwise rotating eddies and the right-hand side of a current core. We have the unique opportunity to test these ideas because the PIES data map both mesoscale circulation and inertial energy distribution in the Ulleung Basin.

Figure 5 illustrates the near-inertial oscillation energy distribution affected by mesoscale circulations in the Ulleung Basin during wintertime. (Watts et al. [this issue] discuss the mesoscale circulation.) The upper row of panels exhibits maps of wintertime-mean circulation (5°C depth Z_5). The middle row of panels maps the corresponding rms amplitudes of band-pass-filtered acoustic echo time within the inertial frequency band. The cutoff of the band-pass filter is ± 1.75 hours from the local inertial period. The combined middle and upper maps exhibit the relationship between the near-inertial energy distribution and the mesoscale current field, as follows.

In the Winter-1 maps, the Ulleung Warm Eddy is strongly developed and a current (the Tsushima Warm Current or “Offshore Branch”) flows along the southern edge. Correspondingly, strong near-inertial oscillations (Figure 5, red regions in the left middle panel) oc-

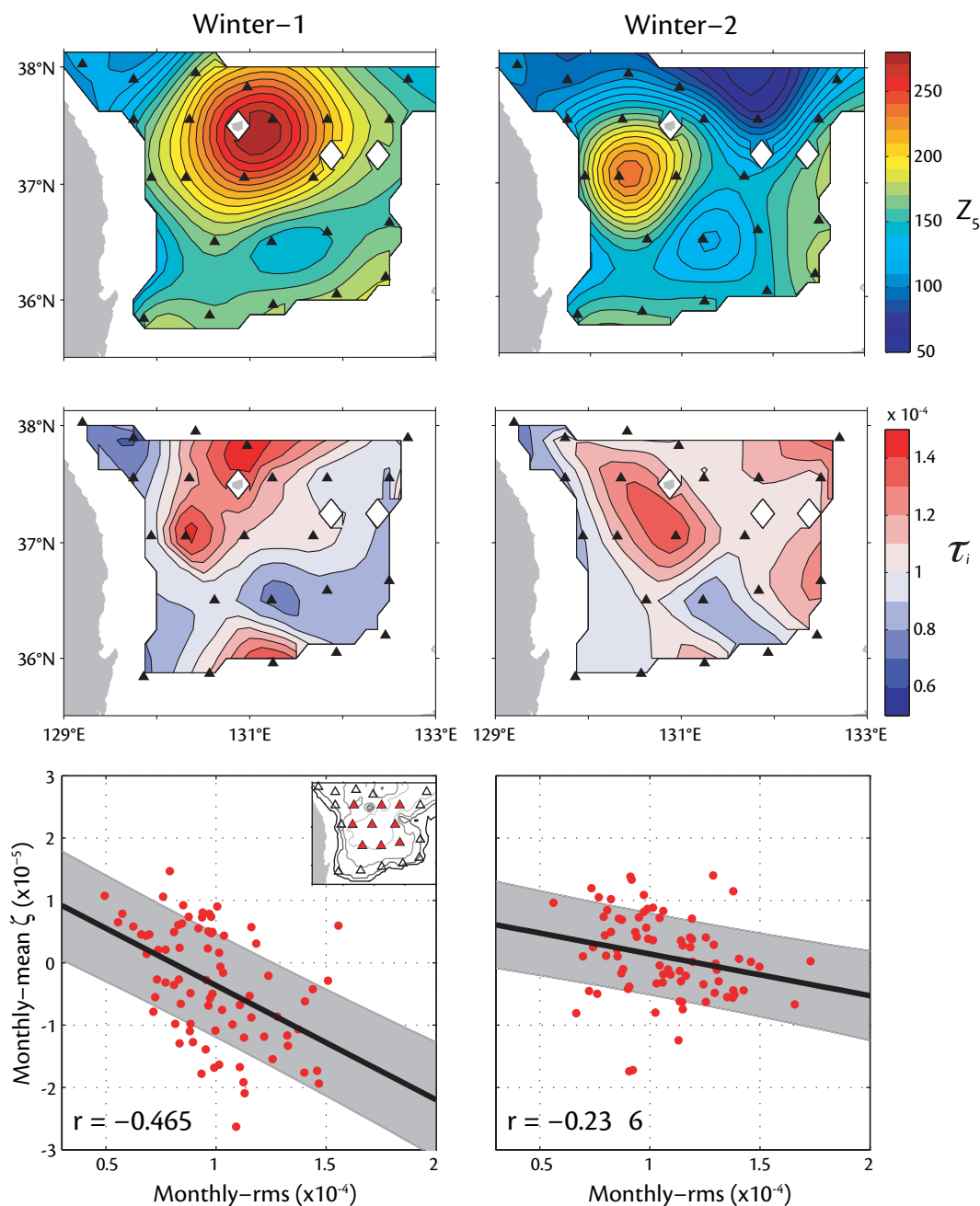


Figure 5. Near-inertial oscillations driven by winter winds are four times more energetic around negative-vorticity features of the mesoscale circulation. (Upper row) Wintertime-mean maps of 5°C depth Z_5 (contour interval 10 m). (Middle row) Wintertime rms amplitude maps of band-pass filtered acoustic echo time in the near-inertial frequency bands (τ_i) (contour interval 10^{-5} s). Solid triangles on each map indicate PIES sites. (Lower row) Scatter plots of monthly rms (τ_i vs. monthly mean ζ at nine PIES sites (red triangles in map) during Winter-1 and Winter-2. Thick solid lines are fitted by least squares; gray-shaded zones indicate error bounds which contain at least 50 percent of the predictions. The correlation coefficients are -0.465 and -0.236 for Winter-1 and Winter-2, respectively. Winter-1 is from November 1, 1999 to March 31, 2000 (first column); Winter-2 is from November 1, 2000 to March 31, 2001 (second column). Both monthly rms τ_i and monthly mean ζ are computed using 30-day segments of time series with 50 percent (15 days) of overlapping.

cur along the northwestern part of the eddy near the Subpolar Front. Another high-energy spot occurs at the southern edge near 131°E along the eastward flowing current.

In the Winter-2 maps, the Ulleung Warm Eddy is small, the Offshore Branch diverts northward along the Oki

Spur on the eastern edge of the domain, and the Subpolar Front meanders south of 38°N. Correspondingly, the strong near-inertial oscillations shift southward near the center of the Ulleung Warm Eddy (Figure 5, red region near 37°N in the middle panel) and are large where it neighbors the Subpolar Front. Another

high-energy spot occurs along 132.5°E along the northward-flowing current.

When compared with ocean circulation patterns, the energy “hotspots” tend to occur in regions with negative relative vorticity. This observation is confirmed by scatter plots of monthly-rms near-inertial band-pass filtered acoustic echo


time versus monthly mean relative vorticity at nine PIES sites (see inset map) during Winter-1 and Winter-2 (lower row of panels in Figure 5). Winter-1 exhibits significant correlation between the two estimates with correlation coefficient $r = -0.465$, while Winter-2 exhibits smaller but still significant correlation with $r = -0.236$. The higher-magnitude correlation observed during Winter-1 may be explained by the strongly developed Ulleung Warm Eddy, which produces a broad negative relative vorticity region in the Ulleung Basin. This calculation supports Kunze's (1985) interpretation because in such locations, the effective inertial frequency is smaller than the local inertial frequency, and hence those regions can trap near-inertial energy. Figure 5 demonstrates that the mesoscale circulation patterns in the Ulleung Basin govern the energy level of near-inertial oscillations in the thermocline.

SUMMARY

Short-period fluctuations such as basin oscillations, internal tides, and near-inertial oscillations are usually investigated as isolated processes. The PIES measured deep pressures and thermocline depth hourly in a two-dimensional array for two years. From these data we could study mesoscale and short-period processes simultaneously. These measurements show that the low-frequency environment in which the high-frequency events occur can drastically alter them. Specifically, in a marginal sea, the inverted barometer approximation is far from perfect and whole-basin oscillations forced by atmospheric and open-ocean pressures cannot be ignored. In addition, horizontal beams of internal tides are

steered and modulated by mesoscale currents and eddy stratification. Moreover, the mesoscale vorticity structure of the eddies can trap and intensify near-inertial oscillations. It is important to understand the coupling of these short- and long-period processes because this coupling should also be prevalent in most other marginal seas.

ACKNOWLEDGEMENTS

The Office of Naval Research "Japan/East Sea DRI" supported this work, including two basic research programs, the Japan/East Sea initiative under grant N000149810246, and the Naval Research Laboratory's Linkages of Asian Marginal Seas under Program Element 0601153N. The Naval Research Laboratory Advanced Graduate Research Program provided additional support for J.W. Book. 

REFERENCES

- Cartwright, D.E. 1982. The tidal signal in inverted echo-sounder records. *Deep-Sea Research* 29:767–784.
- Garrett, C. 1983. Variable sea level and strait flows in the Mediterranean: A theoretical study of the response to meteorological forcing. *Oceanologica Acta* 6:79–87.
- Garrett, C. 2001. What is the "Near-Inertial" band and why is it different from the rest of the internal wave spectrum? *Journal of Physical Oceanography* 31:962–971.
- Griffin, D.A., and K.R. Thompson. 1996. The adjoint method of data assimilation used operationally for shelf circulation. *Journal of Geophysical Research* 101:3,457–3,477.
- Kunze, E. 1985. Near-inertial wave propagation in geostrophic shear. *Journal of Physical Oceanography* 15:544–565.
- Lyu, S.J., and K. Kim. 2005. Subinertial to interannual transport variations in the Korea Strait and their possible mechanisms. *Journal of Geophysical Research* 110:C12,016, doi: 10.1029/2004JC002651.
- Lyu, S.J., K. Kim, and H.T. Perkins. 2002. Atmospheric pressure-forced subinertial variations in the transport through the Korea Strait. *Geophysical Research Letters* 29:1,294, doi: 10.1029/2001GL014366.
- Mitchell, D.A., J.W. Book, K.-I. Chang, M.-S. Suk, W.J. Teague, K.L. Tracey, D.R. Watts, M. Wimbush, and J.-H. Yoon. 2005a. Upper circulation patterns in the southwestern Japan/East Sea. *Deep-Sea Research II* 52:1,617–1,638.
- Mitchell, D.A., W.J. Teague, M. Wimbush, D.R. Watts, and G.G. Sutyrin. 2005b. The Dok Cold Eddy. *Journal of Physical Oceanography* 35:273–288.
- Nam, S.H., S.J. Lyu, Y.H. Kim, K. Kim, J.-H. Park, and D.R. Watts. 2004. Correction of TOPEX/Poseidon altimeter data for nonisostatic sea level response to atmospheric pressure in the Japan/East Sea. *Geophysical Research Letters* 31:L02304, doi: 10.1029/2003GL018487.
- Park, J.-H., and D.R. Watts. 2005a. Response of the southwestern Japan/East Sea to atmospheric pressure. *Deep-Sea Research II* 52:1,671–1,683.
- Park, J.-H., and D.R. Watts. 2005b. Near-inertial oscillations interacting with mesoscale circulation in the southwestern Japan/East Sea. *Geophysical Research Letters* 32:L10611, doi: 10.1029/2005GL022936.
- Park, J.-H., and D.R. Watts. 2006. Internal tides in the southwestern Japan/East Sea. *Journal of Physical Oceanography* 36:22–34.
- Park, J.-H., D.R. Watts, K.L. Tracey, and D.A. Mitchell. 2005. A multi-index GEM technique and its application to the southwestern Japan/East Sea. *Journal of Atmospheric and Oceanic Technology* 22:1,282–1,293.
- Sherwin, T.J., V.I. Vlasenko, N. Stashchuk, D.R. Gus Jeans, and B. Jones. 2002. Along-slope generation as an explanation for some unusually large internal tides. *Deep-Sea Research* 49:1,787–1,799.
- Smith, W.H.F., and D.T. Sandwell. 1997. Global sea-floor topography from satellite altimetry and ship depth soundings. *Science* 277:1,957–1,962.
- Stammer, D., C. Wunsch, and R.M. Ponte. 2000. Dealiasing of global high frequency barotropic motions in altimeter observations. *Geophysical Research Letters* 27:1,175–1,178.
- Teague, W.J., K.L. Tracey, D.R. Watts, J.W. Book, K.-I. Chang, P.J. Hogan, D.A. Mitchell, M.-S. Suk, M. Wimbush, and J.-H. Yoon. 2005. Observed deep circulation in the Ulleung Basin. *Deep-Sea Research II* 52:1,802–1,826.
- Watts, D.R., and H.T. Rossby. 1977. Measuring dynamic heights with inverted echo sounders: Results from MODE. *Journal of Physical Oceanography* 7:345–358.
- Wunsch, C., and D. Stammer. 1997. Atmospheric loading and the oceanic "inverted barometer" effect. *Reviews of Geophysics* 35:79–107.
- Xu, Y., D.R. Watts, and J.-H. Park. 2006a. Improving sea-level estimates from satellite altimetry using in situ measurements in the Japan/East Sea. *Journal of Geophysical Research* (submitted).
- Xu, Y., D.R. Watts, M. Wimbush, and J.-H. Park. 2006b. Basin-mode oscillations in the Japan/East Sea. *Geophysical Research Letters* (submitted).